Inorganic Chemistry

pubs.acs.org/IC Article

Solution Structures of Europium Terpyridyl Complexes with Nitrate and Triflate Counterions in Acetonitrile

Thomas J. Summers, Josiane A. Sobrinho, Ana de Bettencourt-Dias, Shelly D. Kelly, John L. Fulton, and David C. Cantu*



Cite This: Inorg. Chem. 2023, 62, 5207-5218



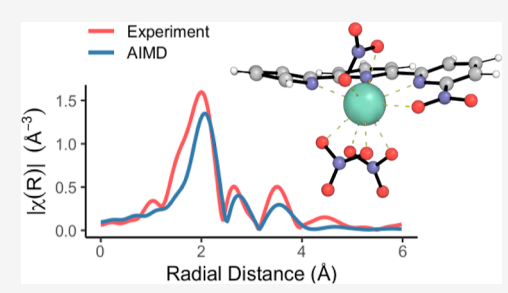
ACCESS

III Metrics & More

Article Recommendations

s Supporting Information

ABSTRACT: Lanthanide—ligand complexes are key components of technological applications, and their properties depend on their structures in the solution phase, which are challenging to resolve experimentally or computationally. The coordination structure of the Eu³⁺ ion in different coordination environments in acetonitrile is examined using ab initio molecular dynamics (AIMD) simulations and extended X-ray absorption fine structure (EXAFS) spectroscopy. AIMD simulations are conducted for the solvated Eu³⁺ ion in acetonitrile, both with or without a terpyridyl ligand, and in the presence of either triflate or nitrate counterions. EXAFS spectra are calculated directly from AIMD simulations and then compared to experimentally measured EXAFS spectra. In acetonitrile



solution, both nitrate and triflate anions are shown to coordinate directly to the Eu³⁺ ion forming either ten- or eight-coordinate solvent complexes where the counterions are binding as bidentate or monodentate structures, respectively. Coordination of a terpyridyl ligand to the Eu³⁺ ion limits the available binding sites for the solvent and anions. In certain cases, the terpyridyl ligand excludes any solvent binding and limits the number of coordinated anions. The solution structure of the Eu-terpyridyl complex with nitrate counterions is shown to have a similar arrangement of Eu³⁺ coordinating molecules as the crystal structure. This study illustrates how a combination of AIMD and EXAFS can be used to determine how ligands, solvent, and counterions coordinate with the lanthanide ions in solution.

■ INTRODUCTION

Lanthanide (Ln) ions bound with organic ligands serve as components in a wide array of applications, such as luminescent optical probes for imaging and sensing, 1-3 magnets for magnetic refrigeration, 4-6 contrast agents for magnetic resonance imaging, 1,2 and single-molecule magnets for quantum information science. 4,7-9 Rare-earth complexes may also function as homogeneous catalysts for a variety of industrially relevant processes including polymerization, dehalogenation, and redox reactions. Due to these application areas, lanthanides have been designated as critical materials, and there is great interest in their separation and recovery from complex mixtures. This is complicated by the similar sizes of the ions and the common oxidation state of +3 in solution, thus making separation and recovery highly active areas of research. 18-26 The ability to resolve the solution structures of Ln-ligand complexes will provide insight and guidance toward not only improving Ln extraction methods but will also facilitate enhancing the magnetic, optical, and catalytic functionalities of Ln-containing materials. However, determining Ln solution structures is particularly challenging both experimentally and computationally; Ln ions have large coordination spheres in which they primarily bind to ligands through ionic interactions, resulting in a multitude of different possible configurations having different numbers of coordinated ligands, counterions, and solvent molecules. Moreover, further complicating the matter, the Ln complexes may exist in an equilibrium between two or more different molecular configurations.²⁷

Although the solid-state structures of many Ln—ligand complexes have been resolved by single-crystal X-ray diffraction, ^{28–35} these may vary from the solution structure, affecting Ln—ligand complex properties of interest. In addition, isolating X-ray quality crystals is not always straightforward. Identifying and characterizing solution structures can be done computationally through electronic structure computations and molecular dynamics simulations ^{36,37} and experimentally through X-ray absorption, NMR spectroscopy, and excitation/emission spectroscopy. ^{38–42} In particular, ab initio molecular dynamics (AIMD) simulations and extended X-ray absorption fine structure (EXAFS) spectroscopy have both been used to successfully characterize several solvated lanthanide and actinide structures. Most of the published research utilizing

Received: January 17, 2023 Published: March 20, 2023





these techniques has centered on the structure of the ion within aqueous solutions, either as a dissolved salt $^{43-59}$ or bound to chelators useful for heavy-metal extraction and biomedical applications. $^{60-70}$ Despite the importance of nonaqueous solutions for several of the applications cited above, far fewer studies examine the ion coordination spheres of such ions in organic solutions beyond resolving the structures of liquid—liquid-extracted ion—ligand complexes. $^{59,68,71-84}$

An Eu complex with terpyNO₂ (6-nitro-2,2'; 6',2"terpyridine) and nitrate (NO₃⁻) was previously isolated³³ in our quest for ligands capable of sensitizing lanthanide-centered emission. We had observed that nitropyridine-carboxylato ligands bind the lanthanide ions through the carboxylate but not through the $-NO_2^{85-88}$ and were thus interested in exploring ligands where the weakly coordinating -NO₂ moiety may bind to the lanthanide ion. We found that this occurs if chelating ligands bearing this functional group are used, such as the tripodal trispicolylamine, bipyridine, and the abovementioned terpyridine. The luminescence properties and nitrocoordination for the Eu-terpyNO2 complex were verified in the solid state by emission spectroscopy and single-crystal X-ray diffraction measurements, respectively. In the complex, Eu is bound to the terpyNO₂ through the three nitrogen atoms of the pyridine rings and one oxygen atom of the -NO2 moiety; the Eu coordination number of 10 and its bicapped square antiprismatic coordination geometry is completed by three NO₃⁻ counteranions bound in a bidentate fashion. The structural changes that might occur when dissolving the complexes were unknown, including how the terpyNO2 ligand might bind. In addition, differences in the binding of the anion NO₃⁻ in crystals grown out of acetonitrile versus the structural arrangements in solution also remained unknown.

In this work, we determine coordination structures of the Eu³⁺ ion within anhydrous acetonitrile solution in the presence of nitrate or the more weakly coordinating triflate (TfO⁻) counteranions and in the presence and absence of the terpyNO₂ ligand. AIMD simulations are used to identify solution structures, and the results are compared to experimental EXAFS spectra. Using AIMD simulations ensures an accurate treatment of the ion environment that accounts for bond formation and the possibility of unexpected chemical reactions. EXAFS provides an accurate measurement of the ligand, anion, and solvent binding in the first shell. By combining these computational and experimental methods, we seek to characterize the structural features of the Eu³⁺ coordination environment in acetonitrile solution.

METHODS

The solution structures of the lanthanide salt and lanthanide ligand complexes were determined using an approach that joins AIMD simulations and EXAFS spectroscopy. For each complex, a theoretical EXAFS spectrum is constructed from AIMD simulation structures, which explicitly account for atomic fluctuations and structural variations. The spectrum generated from AIMD simulation is that which corresponds to the atomic coordinates in the simulation, i.e., the actual spectrum that would be experimentally measured if the sample would have the same atomic coordinates as the simulation. Then, AIMD-generated EXAFS spectra are directly compared to experimental EXAFS spectra. The spectra from simulation and experiment are independent of each other, and no fitting is done to match one to the other. Thus, there is a high likelihood that the simulated atomic coordinates are an accurate representation of the measured sample if the AIMD-generated and experimentally

measured spectra match. This unique approach avoids the more common procedure of mathematically fitting the theoretical EXAFS spectrum of a singular structure to experimental data and thus bypasses assumptions made to fit the data by providing a molecular model to construct the spectra.

Molecular Dynamics Simulations. All our simulations were conducted in periodic boundary conditions with explicit solvent molecules to simulate the liquid phase (see Figure 1). The starting

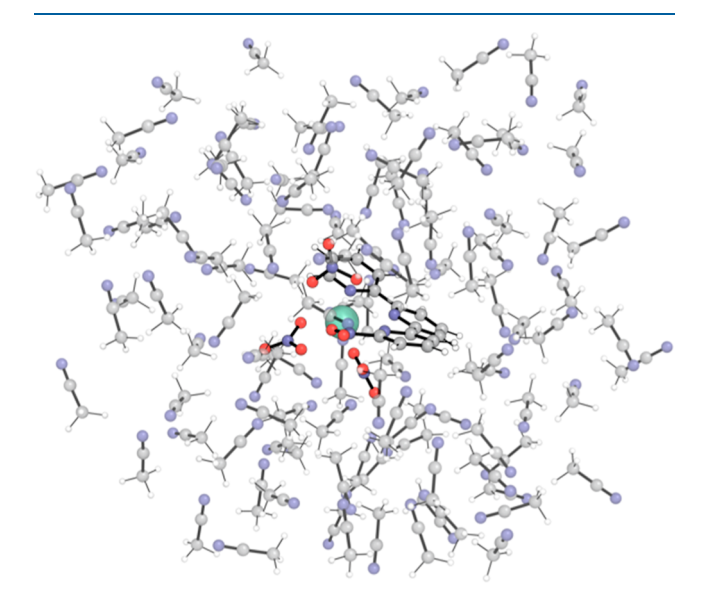


Figure 1. Ball-and-stick illustration of the 698-atom model of $Eu(terpyNO_2)(NO_3)_3$ solvated in acetonitrile. Hydrogen, carbon, nitrogen, oxygen, and Eu atoms are colored white, gray, blue, red, and green, respectively.

structures and box dimensions for the AIMD simulations were obtained from equilibrated classical molecular dynamics simulation structures. The classical simulations were modeled with the OPLS-AA force field so using previously published parameters for acetonitrile, nitrate, triflate, and Eu^{3+} ion. Parameters for the terpyNO₂ ligand are detailed in the Supporting Information. The models were solvated in a periodic cubic box with 109-113 acetonitrile molecules; see Supporting Information for details. The systems were first minimized, followed by 1 ns of NPT simulation to equilibrate the box dimension size using a 1 fs timestep. Temperature and pressure conditions were maintained at 298 K and 1 bar via the Berendsen thermostat and barostats, respectively. 93 Nonbonded interactions were cutoff at 9 Å to accommodate the relatively small model volume, and long-range electrostatic interactions were treated using a particle-mesh Ewald scheme.⁹⁴ All molecules were unrestrained during equilibration in all simulations with one exception: in a control simulation, where Eu³⁺ is coordinated to only acetonitrile molecules, the Eu³⁺ ion and nitrate counterions were restrained to their starting positions to ensure that the ions remained separated. Classical simulations were carried out using GROMACS v2022.2,95 and only for the purpose of providing AIMD simulations a near-equilibrated starting point with a volume corresponding to room temperature at one atmosphere pressure.

Beginning from the equilibrated box dimensions and molecular geometries from the classical molecular dynamics simulations, AIMD simulations were conducted to more accurately characterize the dynamic bond lengths, binding orientations, and denticity of molecules within the coordination spheres of Eu. No position restraints were placed in any AIMD simulation. While some changes in the equilibrium structures of the systems are expected in transitioning from modeling the system classically to quantum mechanically, the equilibrium state is expected to be near the state found from initial refinement by classical molecular dynamics. AIMD computations were performed using the Perdew–Burke–Ernzerhof (PBE) functional, ⁹⁶ as implemented in the CP2K v5.1 program. ^{97,98}

Core electrons were described by Goedecker-Teter-Hutter (GTH) pseudopotentials, 99 and valence electrons were described by a double- ζ valence polarized (DZVP) basis set; 100 the $\rm Ln^{3+}$ ions were described using our LnPP1 pseudopotentials and basis sets. 101 Long-range electrostatics were captured using an auxiliary plane-wave basis set with an 800 Ry cutoff. van der Waals interactions were accounted for using Grimme's D3 corrections with a 6 Å radius cutoff. 102 The simulations were conducted in the NVT ensemble at 298 K with the temperature maintained using the Nosé-Hoover thermostat. 103,104 The systems were simulated at a timestep of 1 fs until at least 10 ps of the system with a stable potential energy and consistent Eu coordination structure was obtained (Figure S2), and the equilibrated trajectory was used to generate radial distribution functions and predict EXAFS spectra.

Theoretical EXAFS spectra. EXAFS spectra for the solution Eu³⁺ structures were predicted from the AIMD simulations. ^{105,106} The coordinates of any C, N, O, F, and S atoms within 8 Å of Eu were extracted from 200 equispaced frames using the final 10 ps of the equilibrated AIMD trajectories. The $\chi(k)$ spectra were computed for each frame using FEFF8.5 software. ^{107–109} We have recently used this approach to predict the EXAFS spectra of Ln³⁺ and Bi³⁺ ions in water solution. ^{44,47,110} FEFF used the default Hedin-Lundqvist exchange correlation potential and used a 6.0 Å cutoff for the self-consistent field calculation. The program was adjusted to include up to 15,000 single- and multiple-scattering paths (increased from the 1200 default), and multiple-scattering paths with up to eight legs were included. Averaging the 200 spectra yields the ensemble-average AIMD-EXAFS spectra reported in this work.

Synthesis of Eu-terpyNO₂ Complexes. To measure the spectra of the Eu³⁺ ion with different counterions in acetonitrile, without ligand, Eu(NO₃)₃ and Eu(TfO)₃ were added to acetonitrile to obtain 0.1 M Eu³⁺ dissolved salt solutions. To measure the spectra of the EuterpyNO₂ complex in acetonitrile with different counterions, equimolar amounts of Eu(NO₃)₃ and terpyNO₂ were mixed in acetonitrile to obtain 0.013 M Eu³⁺ solutions of the ligand-bound Eu³⁺ complex with nitrate as the counteranion; equimolar amounts of Eu(TfO)₃ and terpyNO₂ were mixed in acetonitrile to obtain 0.018 M Eu³⁺ solutions of the ligand-bound Eu³⁺ complex with triflate as the counteranion. The structure of terpyNO₂ is shown in Figure 2. The

Figure 2. Structure of 6-nitro-2,2';6',2"-terpyridine (terpyNO₂).

Eu salts were purchased as the hydrates from VWR and dried for 24 h under reduced pressure and heating to 60 $^{\circ}$ C in an oven. ACS-grade acetonitrile was purchased from VWR and dried by standard methods.

The concentrations of the solutions of the Eu salts in the dried acetonitrile were obtained by titrating with EDTA in the presence of xylenol orange as the indicator. 111 TerpyNO₂ was synthesized as previously reported. 33

Experimental EXAFS Spectra. EXAFS measurements at the Eu L₃-edge (6977 eV) were conducted at the Advanced Photon Source at Argonne National Laboratory (20-BM). The Si (111) monochromator was calibrated to Fe K-edge (7112 eV). The toroidal mirror and slits provided a small X-ray beam less than 0.7×0.7 mm on the samples. Higher harmonic X-rays were minimized using a Rh mirror. Transmission and fluorescence mode measurements were made with ionization chambers and a multi-element Ge solid-state detector, respectively. The Eu3+ salts and dried Eu-terpyNO2 complexes were dissolved in acetonitrile or water immediately prior to EXAFS measurements. The Eu³⁺ salt samples at high (0.1 M) and low (0.013 and 0.018 M) Eu concentration were measured in transmission and fluorescence modes, respectively. Duplicate solutions were deposited in 1 mm glass capillaries. No crystallinity or precipitate were observed in the measured solutions. The high Eu salt samples had transmission edge-steps of approximately 0.35 as expected for 0.1 M solutions. Four measurements of each sample were collected and compared. Comparisons of the quadruplicate measurements showed no significant differences. The measured EXAFS spectra reported are an average of all eight scans (four from each duplicate). Energy calibration was checked by simultaneously measuring an Fe K-edge (7112 eV) with a reference ionization chamber.

Analysis of the EXAFS spectra was performed using Athena from the Demeter v0.9.26 software package. The experimental $\chi(k)$ was extracted from the measured spectrum using a background function with a Fourier filter cutoff distance, $R_{\rm bkg}$, of 1.2 Å. In generating the Fourier transforms, the $\chi(k)$ spectra were weighted with k^2 and windowed using a Hanning function between $2.4 < k < 10.0 \text{ Å}^{-1}$. To compare the experimental and theoretical spectra, only a single parameter, a shift in the edge energy E_0 , was adjusted in the AIMD-EXAFS spectra in order to align the primary oscillations in the $\chi(k)$ spectra to the experimental $\chi(k)$ spectra so that they converge as k approaches zero (Table S3). The amplitude reduction factor S02 was held at 1.0; typically, S02 can vary between 0.7 and 1.0 which could result in as much as 30% over-estimation of the theory relative to the measured spectrum. 113 The mean-square displacement of the halfpath length (s2) values were held at zero. This term in the EXAFS equation accounts for the static and thermal disorder in the shell of atoms surrounding the absorber; both are explicitly accounted for in the AIMD-EXAFS calculations. The experimentally measured EXAFS data are directly compared to theoretical spectra generated from the AIMD trajectory using the FEFF code without further fitting. An exact match between the theory and the measured data is not expected nor required for this study.

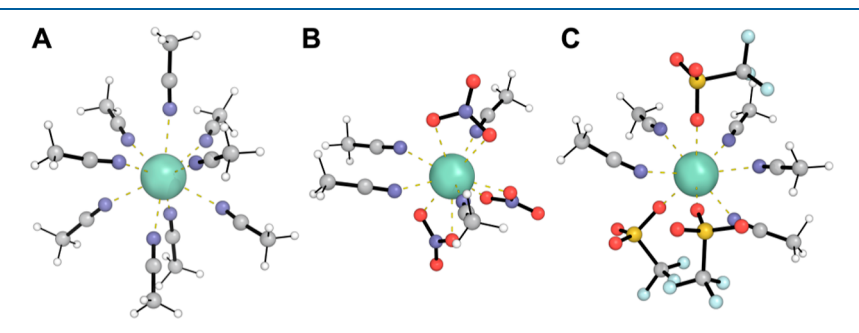


Figure 3. Solvation complexes formed of (a) reference simulation of Eu^{3+} coordinated to only acetonitrile, (b) dissolved $Eu(NO_3)_3$, and (c) dissolved $Eu(TfO)_3$. Hydrogen, carbon, nitrogen, oxygen, sulfur, fluorine, and Eu atoms are colored white, gray, blue, red, yellow, light green, and dark green, respectively. Only the molecules directly coordinating the Eu^{3+} ion are shown for clarity; structures include explicit solvent as indicated in Figure 1.

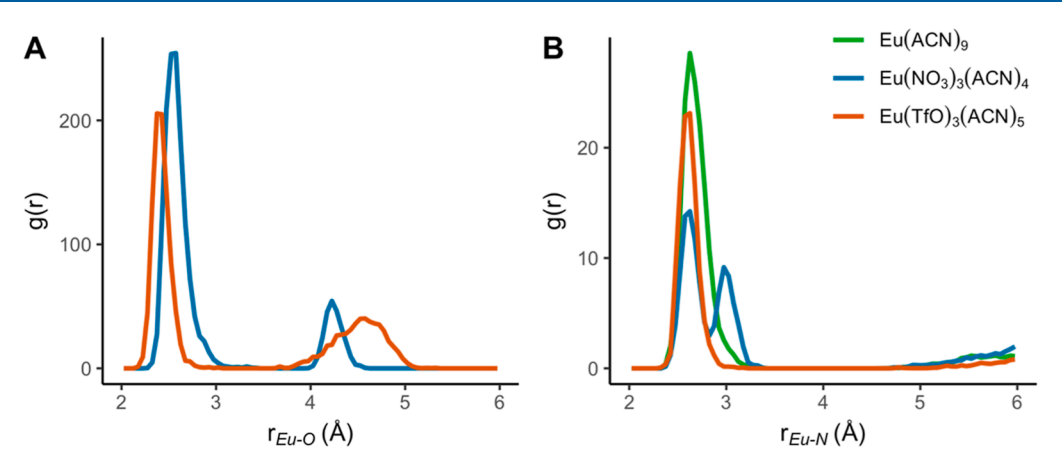


Figure 4. Radial distribution function plots of (a) Eu-O and (b) Eu-N distances for the AIMD simulations of Eu³⁺ coordinated to the solvent and of the dissolved Eu(NO)₃ and Eu(TfO)₃ salts.

■ RESULTS AND DISCUSSION

Solvation of Eu³⁺ Salts in Acetonitrile. We begin by examining the Eu3+ solvation structure for Eu(NO3)3 and Eu(TfO)₃ salts dissolved in acetonitrile. For reference, a simulation of Eu3+ with no counterions in the first and second coordination spheres was carried out to assess Eu³⁺ coordinated to solvent molecules only. Throughout the reference AIMD simulation of the Eu³⁺-acetonitrile coordination structure, nine acetonitrile molecules were coordinated to the metal, mostly in a capped square antiprismatic geometry (Figure 3A). The radial distribution function, g(r), measuring the distance between the Eu and acetonitrile N atoms over the simulation, indicates a well-defined Eu-N distance peak at 2.63 Å (Figure 4B), similar in length to the 2.64 Å distance observed in the complex structure obtained by single-crystal Xray diffraction containing a coordinated acetonitrile. 114 These results largely agree with the findings from previous classical MD simulations, though the classical simulations note an additional acetonitrile involved in the outer sphere solvent exchange⁹² or acting as a capping ligand for a ten-coordinate bicapped square antiprismatic complex.⁸² While there are no indications of this outer sphere acetonitrile from the data of this work (e.g., there is no additional g(r) peak or shoulder beyond 2.63 Å and integration of g(r) is 9.0 up to 4.6 Å, Figure S3), it is feasible that an additional coordinating acetonitrile may appear if a larger time scale were sampled.

In modeling Eu(NO₃)₃ in acetonitrile, the three nitrates readily replace bound acetonitrile molecules and remain in the first coordination sphere of Eu3+ throughout both classical equilibration and AIMD simulation. In agreement with spectroscopic evidence, 115 the nitrates bind to the metal in a bidentate configuration similar to what is observed for aqueous $Eu(NO_3)_3^{116-118}$ Four acetonitrile molecules also bind, forming a ten-coordinate Eu³⁺ complex with a bicapped square antiprismatic geometry (Figure 3B). The Eu-N g(r) peak is at 2.63 Å for the coordinating acetonitrile N, the same distance as for the solvent-only complex, indicating that the metal-binding of the nitrates has no effect on the Eu-acetonitrile bond length (Figure 4B). The g(r) between the Eu and nitrate O atoms indicates two peaks, one at 2.58 Å for the coordinating bidentate O atoms and one at 4.23 Å for the remaining uncoordinated nitrate O atom (Figure 4A). The coordinated Eu-O bond lengths in crystal structures containing coordinated bidentate nitrate generally range from 2.45 to 2.59 Å,

indicating tighter ligand binding in the solid than in the solution-state structures. Both g(r) peaks are sharp, indicating no fluctuation in nitrate denticity in the simulation.

When triflates are present as the counterion instead of nitrates, the triflates similarly replace the bound solvent and remain in the first coordination sphere of Eu³⁺ for both classical and AIMD simulations. This ion pairing in acetonitrile is particularly interesting as the triflate anion does not enter the metal inner coordination sphere of aqueous lanthanide triflate salts due to the higher permittivity of water. 118,122-124 While the complex formed in the equilibrated classical MD simulation included three triflate and six acetonitrile molecules coordinated to the metal, during the AIMD simulation one acetonitrile dissociated, yielding a stable eight-coordinate complex composed of three triflate and five acetonitrile molecules in a mostly square antiprismatic geometry (Figure 3C). The triflates are notably monodentate rather than bidentate. Additionally, the triflates do not change denticity over the measured AIMD simulation, as evidenced by the distinct sharp peak at 2.40 Å for Eu-O g(r) (Figure 4A). The Eu-O distance for triflate is slightly shorter than that for nitrate, likely due to the monodentate configuration of the bound triflate molecules, unlike the bidentate bound nitrate molecules, permitting tighter bonding with the singular triflate O atom; this bond length is also in the 2.31-2.49 Å range of distances observed in crystal structures containing monodentate triflate. $^{33,125-128}$ As with the dissolved Eu(NO₃)₃ salts, the Eu-N distance with triflate as the counterion peaks at 2.63 Å (Figure 4B), reaffirming the lack of an influence between coordinated anion and Eu-acetonitrile bond distance. It is important to note that the Eu-N distance remains relatively constant despite the change in the ion coordination number from nine (pure solvent complex) to ten (dissolved nitrate salt) and eight (dissolved triflate salt). This consistency suggests the Eu-acetonitrile coordination is, as expected, primarily driven by electrostatic interactions, and the number and arrangement of bound solvent molecules will be chiefly influenced by the binding arrangement of other ligands and the combined steric requirements.

To assess the validity of the Eu³⁺ salt solvent structures obtained from the AIMD simulations, a theoretical $\chi(k)$ spectrum was computed for each of the AIMD simulations and compared to experimental spectra of Eu(NO₃)₃ and Eu(TfO)₃ dissolved in acetonitrile. As detailed in the Methods section, this theoretical $\chi(k)$ spectrum comes from averaging the

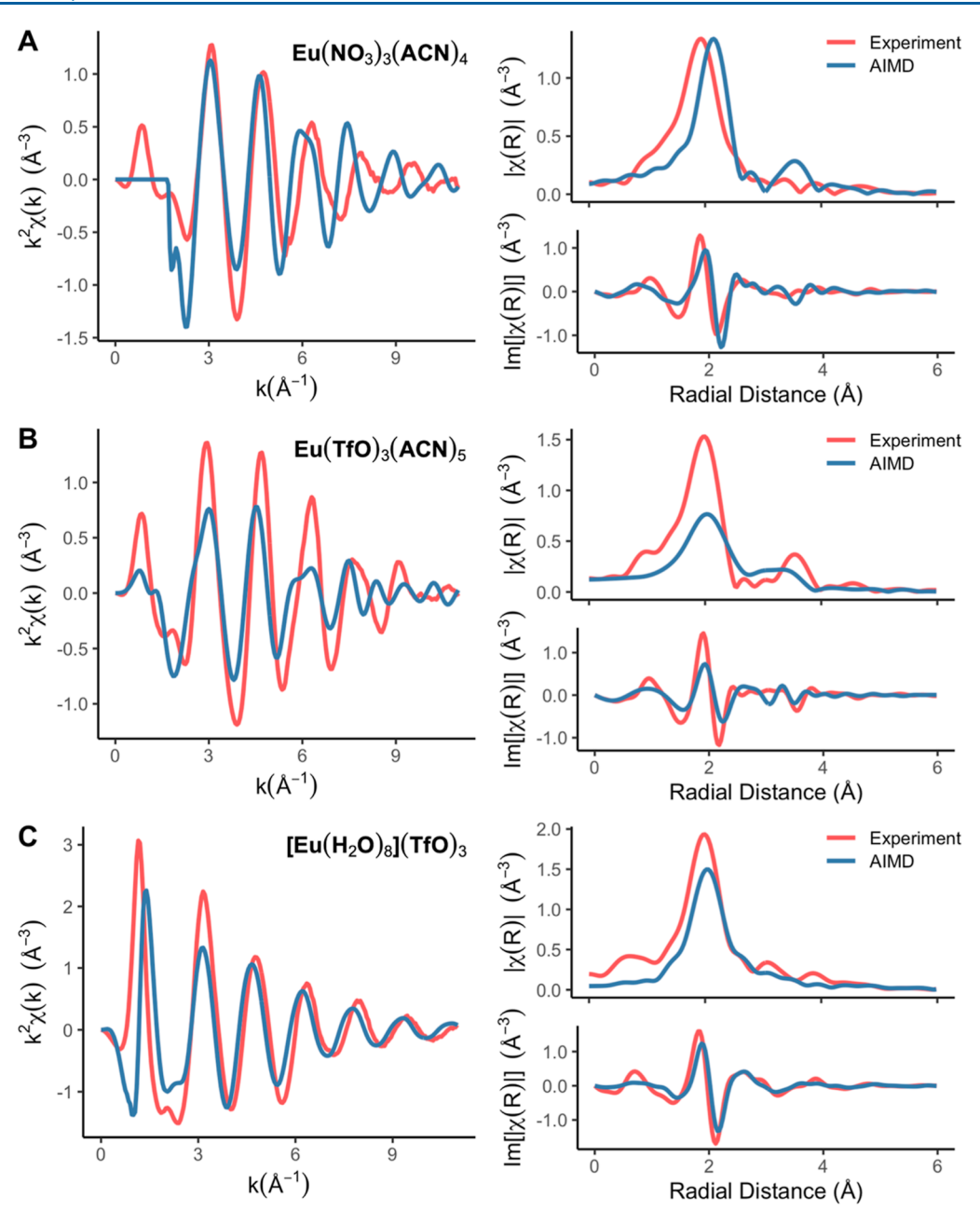


Figure 5. Comparison between experimental (red) and AIMD-derived (blue) EXAFS spectra for the Eu^{3+} L_3 edge of (a) $Eu(NO_3)_3$ dissolved in acetonitrile (ACN), (b) $Eu(TfO)_3$ dissolved in acetonitrile, and (c) $Eu(TfO)_3$ dissolved in water.

theoretical spectra for an ensemble of equilibrium structures from the AIMD simulation. This methodology is different from the more common technique of adjusting the structural parameters (e.g., coordination number, average bond distances, Debye-Waller factors, and asymmetry parameters) for a singular geometry to ideally fit a theoretical EXAFS signal to the experimental spectrum. ¹²⁹ Importantly, our methodology of first obtaining a structure, then computing an expected EXAFS spectrum, was successful in replicating the experimental EXAFS spectra for lanthanide and bismuth aqua ion complexes; ^{44,47,110} this work successfully expands its application toward less homogenous systems.

The experimental and calculated $\chi(k)$ signals for Eu(NO₃)₃ and Eu(TfO)₃ salts dissolved in acetonitrile are illustrated in Figure 5 alongside their respective k^2 -weighted Fourier transform spectra. There is general agreement between the

experimental and theoretical spectra in the frequency and shape of the $\chi(k)$ oscillations, even with the absence of fitting and the relative complexity of the modeled systems. This indicates that the identities and general spatial positioning of the molecules within the first coordination sphere of the metal are consistent with the measured spectra. The Fourier transform results indicate that the experimental distance between Eu³⁺ and its coordinated atoms for solvated Eu(NO₃)₃ is slightly shorter than what is observed in the AIMD simulation, with a difference in peaks of 0.21 Å (0.09 Å for the imaginary component $Im[|\chi(R)|]$). This difference is smaller for the Eu(TfO)₃ system, where the difference in peaks is only 0.03 Å (0.03 Å for the imaginary component). Some of the features arising by scattering from the C, N, and S atoms covalently bound to the coordinating atoms are captured in the

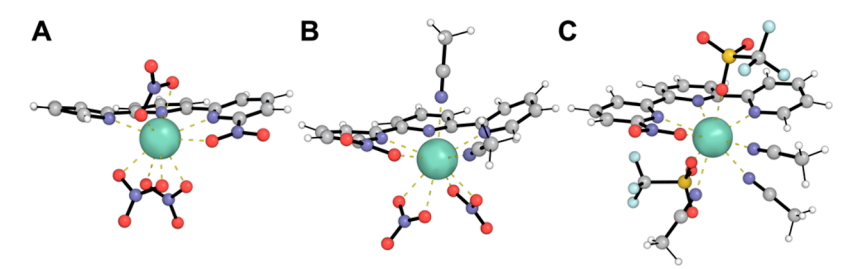


Figure 6. Modeled solvation complexes of Eu³⁺ bound to the terpyNO₂ ligand along with (a) nitrates, (b) nitrates and solvent, or (c) triflates and solvent. Hydrogen, carbon, nitrogen, oxygen, sulfur, fluorine, and Eu atoms are colored white, gray, blue, red, yellow, light green, and dark green, respectively. Only the molecules directly coordinated to the Eu³⁺ ion are shown for clarity; structures include explicit solvent as illustrated in Figure

radial distance range >3 Å, such as the peaks near 3.5 Å for $Eu(TfO)_3$.

We expect that sampling over longer time scales, outside the range of AIMD, to ensure inclusion of more structural conformations would further improve the similarity between theoretical and experimental spectra. Another possibility is that, despite careful drying to ensure anhydrous acetonitrile (see Methods), water contamination could explain the discrepancies between the experimental and predicted spectra in Figure 5A,B. Water can absorb into organic solvents, even under controlled humidity conditions. ¹³⁰

As further evidence for the proposed solution structures, the spectra were compared against the theoretical EXAFS spectra predicted for the Eu³+ ion coordinated to only acetonitrile molecules (Figures S5 and S6). The greater similarity between the experimental and theoretical EXAFS spectrum for the solvated salt compared to Eu³+ coordinated to only acetonitrile (as measured by the residual sum of squares of the $\chi(k)$ signals) supports the predictions from the AIMD simulations that both nitrates and triflates are coordinated to the metal when dissolved in acetonitrile solvent.

To reaffirm that the triflates are within the first coordination sphere for Eu³⁺ when solvated in acetonitrile but not when in water, the EXAFS spectrum for aqueous Eu(TfO)₃ was also measured. A theoretical EXAFS spectrum was constructed using the AIMD simulation geometries from a previously published study modeling aqueous LnCl₃ salts.⁴⁴ Although the study used chloride instead of triflate as the counterion, the chloride displayed the same solvation behavior presumed for aqueous triflate by consistently remaining outside the first and second coordination spheres. In the AIMD simulation, the Eu³⁺ coordinates to eight water molecules in a square antiprismatic geometry. The experimental and AIMD-derived spectra for the Eu³⁺ octa—aqua complex are shown in Figure 5. There is good agreement in the frequency and shape of the $\chi(k)$ oscillations between the experimental and theoretical spectra, indicating accurate modeling of the metal-water bond lengths and geometry. The Fourier transform further confirms this with only a 0.06 Å difference in the first coordination sphere peaks (0.06 Å for the imaginary component peak). Combining this information with the EXAFS spectra for Eu(TfO)₃ dissolved in acetonitrile, the results indicate that the higher permittivity and stronger solvation ability of water leads to the complete dissociation of the salt, but the lower permittivity of acetonitrile leads to the triflates remaining in the first coordination shell.

Solvation of Eu³⁺-Terpyridyl Ligand Complexes in Acetonitrile. After characterizing the structure of Eu³⁺ salts dissolved in acetonitrile, we now examine the effect complex-

ation with the terpyNO₂ ligand (Figure 2) has on the Eu³⁺ coordination structure in solution. The addition of terpyNO₂ to Eu³⁺ nitrate and triflate salts in acetonitrile resulted in the formation of Eu-terpyNO₂ complexes in acetonitrile solution with either nitrate or triflate counterions; a terpyNO₂ molecule displaced solvent molecules to coordinate the Eu³⁺ ion. The EXAFS spectra of Eu³⁺ nitrate or triflate with and without terpyNO₂ in acetonitrile show clear changes in the coordination structure of the Eu³⁺ ion (Figure S7). This section details the AIMD simulations, and comparing AIMD-predicted EXAFS spectra to measured EXAFS spectra confirms the binding of terpyNO₂ to Eu³⁺ in acetonitrile solution with nitrate or triflate counterions.

In modeling the Eu-terpyNO2 complex with nitrates in solution as the counterion, the nitrates readily replaced the coordinated acetonitrile molecules and remained bound to the Eu³⁺ ion alongside the bound ligand. AIMD simulations for two equilibrated starting structures were conducted, one where all three nitrates were coordinated to the metal in a bidentate configuration like in the geometry obtained by crystallography (Figure 6A) and one where two nitrates were bidentate and one was monodentate, as suggested by classical molecular dynamics simulations; this allows one acetonitrile molecule to also coordinate with the Eu3+ ion. During the AIMD simulation, the monodentate nitrate of the latter starting structure immediately dissociated from the metal, allowing the bound acetonitrile molecules to reorient and form a stable complex with two bidentate nitrates and two acetonitrile molecules in the first coordination sphere (Figure 6B), with the third nitrate in the second or third coordination sphere.

Both solvated Eu-terpyNO₂ complexes contain a tencoordinate Eu³⁺ with the bound atoms arranged in a bicapped square antiprismatic geometry. As was reported for the X-ray crystal structure, 33 the Eu3+ does not fit comfortably within the terpyNO2 cavity, causing the Eu3+ ion to be offset from the ideal plane of the terpyNO2 and leading to torsional distortion of the ligand rings. In solution, the Eu is located on average 0.56 ± 0.35 Å below the plane spanned by the central terpyNO2 ring, which is slightly shorter than the 0.652 Å distance observed in the X-ray crystal structure. While the torsional distortion between adjacent terpyNO2 rings is relatively consistent in the solid-state structure (7.89 and 8.03° between the central ring and either the adjacent ring with or without the $-NO_2$ functional group, respectively), they are not similar in solution. The presence of the -NO2 moiety notably reinforces the planarity of adjacent rings, leading to an average torsion angle between the central ring and the ring containing $-NO_2$ of $3.3 \pm 10.9^{\circ}$ compared to the average 15.0 \pm 11.5° angle observed between the other ring pair.

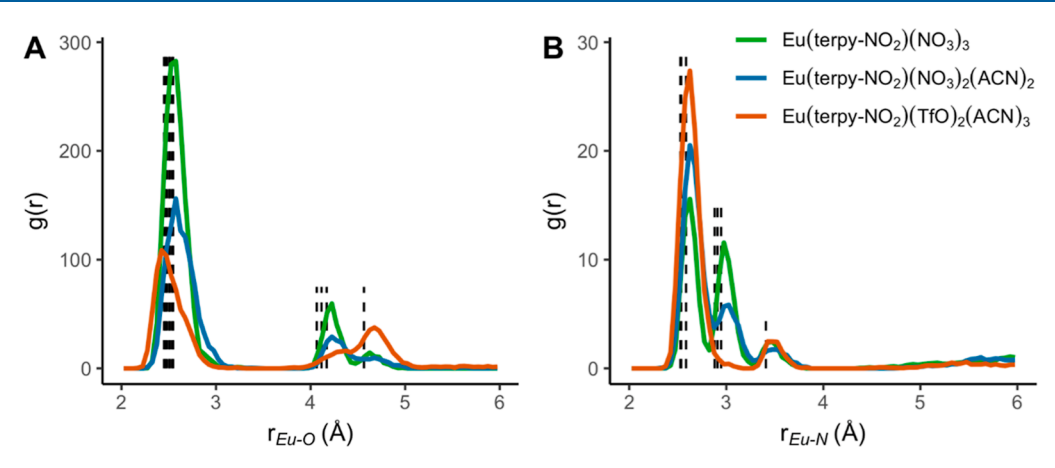


Figure 7. Radial distribution function plots of (a) Eu-O and (b) Eu-N distances for the simulations of the ligand-bound Eu³⁺ coordinated to the solvent and different anions. Black dashed lines indicate distances observed in the X-ray crystal structure of Eu(terpy-NO₂)(NO₃)₃.

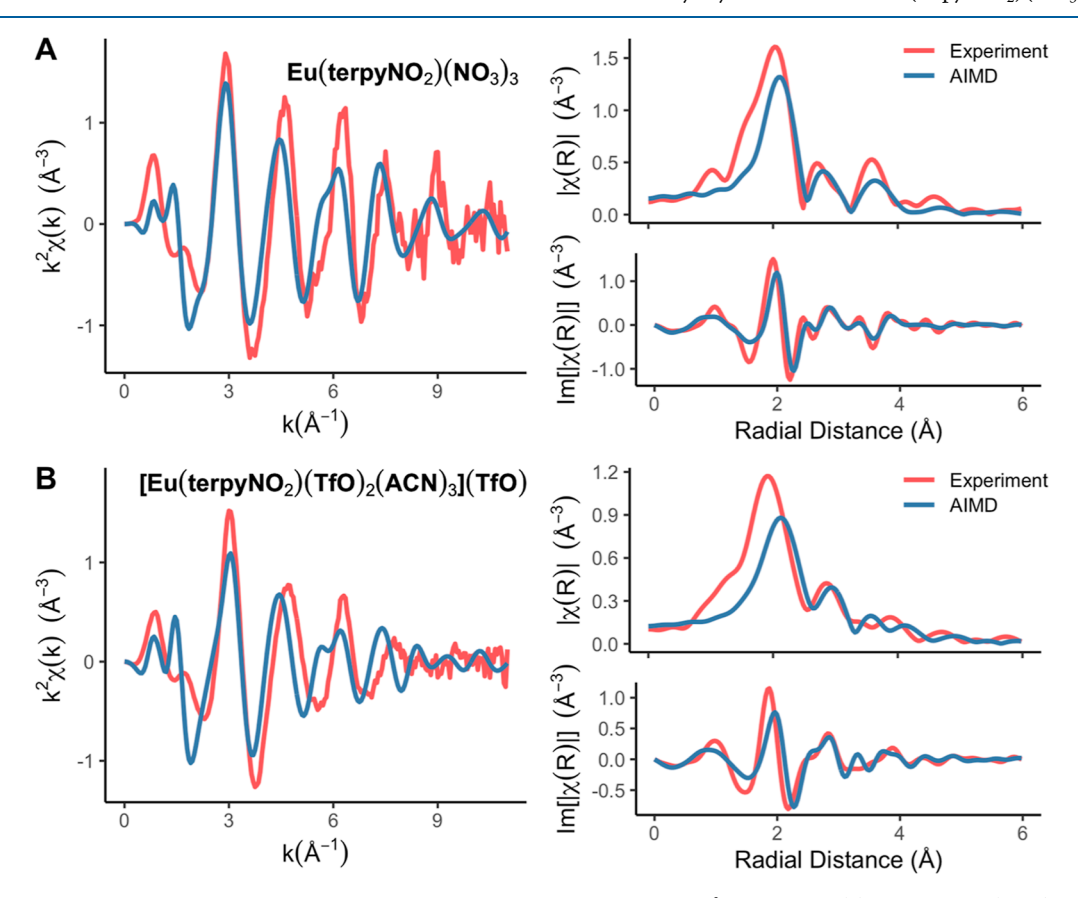


Figure 8. Comparison between experimental and AIMD-derived EXAFS spectra for the Eu^{3+} L_3 edge of (a) dissolved $Eu(NO_3)_3$ complexed with terpyNO₂ and (b) dissolved $Eu(TfO)_3$ complexed with terpyNO₂.

The first Eu-N g(r) peak is at 2.63 Å for both solution structures (Figures 7B, S8), which is the same distance seen for the dissolved salts but is slightly longer than the average 2.55 Å bond length observed in the crystalline structure. The distinctly sharp g(r) peak indicates no significant difference between the Eu-N bond length of bound acetonitrile and terpyNO₂. The first Eu-O g(r) is at 2.58 Å for both solution structures (Figures 7A, S8), which is the same as the dissolved Eu(NO₃)₃ salt. Although subtle, the Eu-N and Eu-O peaks for the complex with only two nitrates are slightly broadened compared to the three-nitrate complex, suggesting that, as more nitrates bind to the Eu³⁺, the complex becomes slightly more rigid.

When the nitrate anions are substituted with triflates, the triflates remain in the first coordination sphere of the terpyNO₂-bound Eu³⁺ ion. The complex formed in the equilibrated classical MD simulation included all three triflates in the first coordination sphere, though one triflate dissociated during the beginning of the AIMD simulation. The resulting stable complex contains two triflates and three acetonitrile molecules in the first coordination sphere arranged in a nine-coordinate capped square antiprismatic geometry, with the third anion in the second or third coordination spheres (Figure 6C). As seen in the dissolved Eu(TfO)₃ simulation, the triflates are monodentate instead of bidentate and have a shorter Eu—O distance (peak at 2.43 Å, Figure 7A) compared to the

nitrates. The first Eu–O peak for the triflates also contains a shoulder near 2.6 Å attributable to the coordinated oxygen atom of the nitro functional group of the terpyNO₂; in the crystal structure, this distance is 2.545 Å.³³ The Eu–N distance with triflate sharply peaks at 2.63 Å, the same as the other salt and ligand complexes.

The theoretical EXAFS spectra for the Eu-terpyNO2 complexes were computed from the AIMD simulations, and the spectra are compared to experimental EXAFS data in Figure 8. As two different structures were modeled for the metal complex with nitrates present (Figure 6A,B), the difference between each of their EXAFS spectra and the experimental spectrum was examined (Figure S9), revealing greater similarity between the experiment and the complex with all three nitrates bound (Figure 6A). For both cases of the complex with nitrates and triflates present, there is excellent agreement between the experimental and AIMD-derived spectra in the frequency and shape of the $\chi(k)$ oscillations. This is further supported by the effective replication of most of the features and amplitudes in the Fourier transform of the signals. The AIMD simulation of the complex with coordinated nitrates accurately reproduces the experimental bond length between the Eu³⁺ and coordinated atoms, with a difference in the primary peak of the Fourier-transformed signal of only 0.09 Å (0.06 Å for the imaginary component). This metal-atom distance for the triflate complex is longer in the AIMD simulations relative to that in the experiment by 0.21 Å (0.09 Å for the imaginary component). Overall, the similarity between the experimental and theoretical EXAFS spectra supports the proposed solution structures of the Eu-terpyNO2 complexes in acetonitrile.

Considering the collective results of this work, the consistency in the Eu-N and Eu-O bond lengths among solvated salt and ligand-bound complexes, irrespective of differing coordination numbers and net charge, highlights how the lanthanide coordination is primarily driven by electrostatic interactions rather than chemical bonding in acetonitrile. Similarly, the lack of a difference between the Eu-N lengths of acetonitrile and terpyNO2 suggests that the affinity for the metal to bind to the ligand over the solvent is predominantly due to the chelate effect. Because of these properties, the number and arrangement of coordinated species can be tuned based on the design of the ligand and the choice of the anion and solvent. From this work, the use of acetonitrile instead of water as solvent permitted triflate to act as a coordinating anion. Likewise, the difference between the smaller, bidentate nitrates versus the bulkier, monodentate triflates for the EuterpyNO₂ complex affected the number of coordinated anions, the inclusion of the solvent in the first coordination sphere, the final coordination geometry, and the net charge on the complex ion.

This work focuses on how a ligand (terpyNO $_2$) changes the Eu $^{3+}$ coordination structure with different counterions (nitrate, triflate) in acetonitrile solution, and how AIMD and EXAFS are successfully combined to resolve the structure of Ln–ligand complexes in solution. Future research with the same methodology, focusing on other Ln $^{3+}$ ions, counterions, solvents, and ligands, will generate a combined theoretical and experimental approach to enable drawing universal conclusions on the intricate role that ligands, counterions, and solvent molecules play in the coordination structures of lanthanide ions in solution.

CONCLUSIONS

We used a unique approach that coupled AIMD simulations with experimental EXAFS spectra to characterize different structures of the Eu3+ ion within an anhydrous acetonitrile solution, which are otherwise not easily discernible. The AIMD simulation of the dissolved Eu(NO₃)₃ salt formed a tencoordinate solvated complex where all three nitrates retain a bidentate configuration bound with the metal. When the Eu(TfO)₃ salt was dissolved in acetonitrile, it formed an eightcoordinate complex with the three TfO⁻ anions within the first coordination sphere in a monodentate configuration. Conversely, when Eu(TfO)₃ was dissolved in water, TfO⁻ anions remained outside the first coordination sphere. The complexation of Eu3+ to the terpyNO2 ligand limited the available coordination sites for the solvent and anions. If nitrates were present as the counterion, they preferentially coordinated over the solvent to form a ten-coordinate complex. If triflates were present as the counterion, their larger size and monodentate coordination hindered all three counterions from binding to the Eu³⁺ ion, resulting in a nine-coordinate complex with only two of the three triflates bound. Measured EXAFS spectra were compared against AIMD-generated EXAFS spectra of the dissolved salts as evidence in support of the proposed solvated

The findings of this work underpin how the choice of ligand, solvent, and counterion all play significant roles in crafting the final coordination structures of solvated lanthanide complexes. As the coordination of anions and solvent can alter the spectroscopic properties of lanthanide—ligand complexes (relevant in imaging or sensing) or accessibility of the lanthanide ion (relevant in catalysis or separations), developing methods such as the one outlined here to reliably predict experimental solvation structures will further advance the design of lanthanide complexes for societally relevant applications.

ASSOCIATED CONTENT

Supporting Information

The Supporting Information is available free of charge at https://pubs.acs.org/doi/10.1021/acs.inorgchem.3c00199.

AIMD model information; classical molecular dynamics parameters; Figure S1: schematic of the atomtypes for the terpyNO $_2$ ligand and partial atomic charges; OPLS parameter information for the terpyNO $_2$ ligand; Figure S2: potential energy plots of AIMD simulations; example FEFF input file; correction of calculated potentials; Figures S3 - S9: radial distribution function plots and overlays of EXAFS spectra from AIMD and experiment, for various cases of the Eu $^{3+}$ ion, with or without the terpyNO $_2$ ligand, with an NO $_3$ or TfO counterion, dissolved in acetonitrile (PDF)

AUTHOR INFORMATION

Corresponding Author

David C. Cantu — Department of Chemical and Materials Engineering, University of Nevada, Nevada 89557-0388, United States; orcid.org/0000-0001-9584-5062; Email: dcantu@unr.edu

Authors

Thomas J. Summers — Department of Chemical and Materials Engineering, University of Nevada, Nevada 89557-0388, United States; orcid.org/0000-0002-4243-6078

Josiane A. Sobrinho – Department of Chemistry, University of Nevada, Nevada 89557-0705, United States

Ana de Bettencourt-Dias — Department of Chemistry, University of Nevada, Nevada 89557-0705, United States; occid.org/0000-0001-5162-2393

Shelly D. Kelly – X-ray Science Division, Argonne National Laboratory, Argonne, Illinois 60439-4801, United States; orcid.org/0000-0001-8996-628X

John L. Fulton — Physical Sciences Division, Pacific Northwest National Laboratory, Richland, Washington 99352, United States; Oorcid.org/0000-0001-9361-9803

Complete contact information is available at: https://pubs.acs.org/10.1021/acs.inorgchem.3c00199

Notes

The authors declare no competing financial interest.

ACKNOWLEDGMENTS

This material is based upon work supported by the U.S. Department of Energy (DOE), Office of Science, Office of Basic Energy Sciences under Award DE-SC0022178 (to A.d.B.D. and D.C.C.). D.C.C. acknowledges support from the National Science Foundation (Award 2041914). Work by J.L.F. was supported under project 16248 funded by the U.S. Department of Energy (DOE), Office of Science, Office of Basic Energy Sciences, Division of Chemical Sciences, Geosciences, and Biosciences. This research used resources of the Advanced Photon Source, a U.S. Department of Energy (DOE) Office of Science user facility operated for the DOE Office of Science by Argonne National Laboratory under Contract no. DE-AC02-06CH11357. This research used resources of the National Energy Research Scientific Computing Center, a DOE Office of Science User Facility supported by the Office of Science of the U.S. Department of Energy under Contract no. DE-AC02-05CH11231 using NERSC award BES-ERCAP0021496.

REFERENCES

- (1) Heffern, M. C.; Matosziuk, L. M.; Meade, T. J. Lanthanide Probes for Bioresponsive Imaging. *Chem. Rev.* **2014**, *114*, 4496–4539.
- (2) Comby, S.; Surender, E. M.; Kotova, O.; Truman, L. K.; Molloy, J. K.; Gunnlaugsson, T. Lanthanide-Functionalized Nanoparticles as MRI and Luminescent Probes for Sensing and/or Imaging Applications. *Inorg. Chem.* **2014**, *53*, 1867–1879.
- (3) de Bettencourt-Dias, A. Modern Applications of Lanthanide Luminescence; *Springer Series on Fluorescence*; Springer International Publishing: Cham, Switzerland, 2023; Vol. 19.
- (4) Yu, H.; Yang, J.-X.; Han, J.-Q.; Li, P.-F.; Hou, Y.-L.; Wang, W.-M.; Fang, M. Tetranuclear Lanthanide Complexes Showing Magnetic Refrigeration and Single Molecule Magnet Behavior. *New J. Chem.* **2019**, *43*, 8067–8074.
- (5) Zheng, Y.-Z.; Zhou, G.-J.; Zheng, Z.; Winpenny, R. E. P. Molecule-Based Magnetic Coolers. *Chem. Soc. Rev.* **2014**, *43*, 1462–1475.
- (6) Liu, J.-L.; Chen, Y.-C.; Guo, F.-S.; Tong, M.-L. Recent Advances in the Design of Magnetic Molecules for Use as Cryogenic Magnetic Coolants. *Coord. Chem. Rev.* **2014**, *281*, 26–49.
- (7) Woodruff, D. N.; Winpenny, R. E. P.; Layfield, R. A. Lanthanide Single-Molecule Magnets. *Chem. Rev.* **2013**, *113*, 5110–5148.

- (8) Zhu, Z.; Guo, M.; Li, X.-L.; Tang, J. Molecular Magnetism of Lanthanide: Advances and Perspectives. *Coord. Chem. Rev.* **2019**, *378*, 350–364
- (9) Dey, A.; Kalita, P.; Chandrasekhar, V. Lanthanide(III)-Based Single-Ion Magnets. ACS Omega 2018, 3, 9462–9475.
- (10) Tsurugi, H.; Mashima, K. Renaissance of Homogeneous Cerium Catalysts with Unique Ce(IV/III) Couple: Redox-Mediated Organic Transformations Involving Homolysis of Ce(IV)–Ligand Covalent Bonds. J. Am. Chem. Soc. 2021, 143, 7879–7890.
- (11) Gao, W.; Cui, D. Highly Cis-1,4 Selective Polymerization of Dienes with Homogeneous Ziegler—Natta Catalysts Based on NCN-Pincer Rare Earth Metal Dichloride Precursors. *J. Am. Chem. Soc.* **2008**, *130*, 4984–4991.
- (12) Yin, H.; Carroll, P. J.; Anna, J. M.; Schelter, E. J. Luminescent Ce(III) Complexes as Stoichiometric and Catalytic Photoreductants for Halogen Atom Abstraction Reactions. *J. Am. Chem. Soc.* **2015**, *137*, 9234–9237.
- (13) Zimmermann, M.; Törnroos, K. W.; Anwander, R. Cationic Rare-Earth-Metal Half-Sandwich Complexes for the Living Trans-1,4-Isoprene Polymerization. *Angew. Chem., Int. Ed.* **2008**, *47*, 775–778.
- (14) Mikami, K.; Terada, M.; Matsuzawa, H. "Asymmetric" Catalysis by Lanthanide Complexes. *Angew. Chem., Int. Ed.* **2002**, *41*, 3554–3572.
- (15) Qiao, Y.; Schelter, E. J. Lanthanide Photocatalysis. Acc. Chem. Res. 2018, 51, 2926–2936.
- (16) Barisic, D.; Buschmann, D. A.; Schneider, D.; Maichle-Mössmer, C.; Anwander, R. Rare-Earth-Metal Pentadienyl Half-Sandwich and Sandwich Tetramethylaluminates—Synthesis, Structure, Reactivity, and Performance in Isoprene Polymerization. *Chem. Eur. J.* **2019**, 25, 4821–4832.
- (17) Shi, X.; Nishiura, M.; Hou, Z. C-H Polyaddition of Dimethoxyarenes to Unconjugated Dienes by Rare Earth Catalysts. *J. Am. Chem. Soc.* **2016**, *138*, 6147–6150.
- (18) O'Connell-Danes, J. G.; Ngwenya, B. T.; Morrison, C. A.; Love, J. B. Selective Separation of Light Rare-Earth Elements by Supramolecular Encapsulation and Precipitation. *Nat. Commun.* **2022**, *13*, 4497.
- (19) Li, X.-Z.; Zhou, L.-P.; Yan, L.-L.; Dong, Y.-M.; Bai, Z.-L.; Sun, X.-Q.; Diwu, J.; Wang, S.; Bünzli, J.-C.; Sun, Q.-F. A Supramolecular Lanthanide Separation Approach Based on Multivalent Cooperative Enhancement of Metal Ion Selectivity. *Nat. Commun.* **2018**, *9*, 547.
- (20) Li, Z.; Binnemans, K. Hydration Counteracts the Separation of Lanthanides by Solvent Extraction. *AIChE J.* **2020**, *66*, No. e16545.
- (21) Higgins, R. F.; Ruoff, K. P.; Kumar, A.; Schelter, E. J. Coordination Chemistry-Driven Approaches to Rare Earth Element Separations. *Acc. Chem. Res.* **2022**, *55*, 2616–2627.
- (22) Daumann, L. J. A. Natural Lanthanide-Binding Protein Facilitates Separation and Recovery of Rare Earth Elements. ACS Cent. Sci. 2021, 7, 1780–1782.
- (23) Sun, P.; Binter, E. A.; Liang, Z.; Brown, M. A.; Gelis, A. V.; Benjamin, I.; Bera, M. K.; Lin, B.; Bu, W.; Schlossman, M. L. Antagonistic Role of Aqueous Complexation in the Solvent Extraction and Separation of Rare Earth Ions. *ACS Cent. Sci.* **2021**, *7*, 1908–1918.
- (24) Baldwin, A. G.; Ivanov, A. S.; Williams, N. J.; Ellis, R. J.; Moyer, B. A.; Bryantsev, V. S.; Shafer, J. C. Outer-Sphere Water Clusters Tune the Lanthanide Selectivity of Diglycolamides. *ACS Cent. Sci.* **2018**, *4*, 739–747.
- (25) Lovering, K.; Nayak, S.; Bu, W.; Uysal, A. The Role of Specific Ion Effects in Ion Transport: The Case of Nitrate and Thiocyanate. *J. Phys. Chem. C* **2020**, *124*, 573–581.
- (26) Picayo, G. A.; Etz, B. D.; Vyas, S.; Jensen, M. P. Characterization of the ALSEP Process at Equilibrium: Speciation and Stoichiometry of the Extracted Complex. *ACS Omega* **2020**, *5*, 8076–8089.
- (27) Bünzli, J.-C. G. Review: Lanthanide Coordination Chemistry: From Old Concepts to Coordination Polymers. *J. Coord. Chem.* **2014**, 67, 3706–3733.

- (28) de Bettencourt-Dias, A.; Beeler, R. M.; Zimmerman, J. R. Anion- π and H-Bonding Interactions Supporting Encapsulation of $[\text{Ln(NO_3)}_{6/5}]^{3-/2-}$ (Ln = Nd, Er) with a Triazine-Based Ligand. *J. Am. Chem. Soc.* **2019**, *141*, 15102–15110.
- (29) de Bettencourt-Dias, A.; Beeler, R. M.; Zimmerman, J. R. Secondary-Sphere Chlorolanthanide(III) Complexes with a 1,3,5-Triazine-Based Ligand Supported by Anion— π , π — π , and Hydrogen-Bonding Interactions. *Inorg. Chem.* **2020**, *59*, 151–160.
- (30) Fitzgerald, M.; Emge, T. J.; Brennan, J. G. Chalcogen-Rich Lanthanide Clusters with Fluorinated Thiolate Ligands. *Inorg. Chem.* **2002**, *41*, 3528–3532.
- (31) Charbonnière, L. J.; Ziessel, R.; Montalti, M.; Prodi, L.; Zaccheroni, N.; Boehme, C.; Wipff, G. Luminescent Lanthanide Complexes of a Bis-Bipyridine-Phosphine-Oxide Ligand as Tools for Anion Detection. J. Am. Chem. Soc. 2002, 124, 7779–7788.
- (32) Armaroli, N.; Accorsi, G.; Barigelletti, F.; Couchman, S. M.; Fleming, J. S.; Harden, N. C.; Jeffery, J. C.; Mann, K. L. V.; McCleverty, J. A.; Rees, L. H.; Starling, S. R.; Ward, M. D. Structural and Photophysical Properties of Mononuclear and Dinuclear Lanthanide(III) Complexes of Multidentate Podand Ligands Based on Poly(Pyrazolyl)Borates. *Inorg. Chem.* 1999, 38, 5769–5776.
- (33) de Bettencourt-Dias, A.; Bauer, S.; Viswanathan, S.; Maull, B. C.; Ako, A. M. Unusual Nitro-Coordination of Europium(III) and Terbium(III) with Pyridinyl Ligands. *Dalton Trans.* **2012**, *41*, 11212–11218.
- (34) de Bettencourt-Dias, A.; Zimmerman, J. R. New k^1,k^1 -Benzoato-Bridged Complexes of Eu(III) and Tb(III) with a Triazine-Benzamide Ligand. *Main Group Chem.* **2012**, *11*, 31–44.
- (35) Monteiro, J. H. S. K.; de Bettencourt-Dias, A.; Mazali, I. O.; Sigoli, F. A. The Effect of 4-Halogenobenzoate Ligands on Luminescent and Structural Properties of Lanthanide Complexes: Experimental and Theoretical Approaches. *New J. Chem.* **2015**, 39, 1883–1891.
- (36) Cantu, D. C. Predicting lanthanide coordination structures in solution with molecular simulation. In *Methods in Enzymology*; Cotruvo, J. A., Ed.; *Rare-Earth Element Biochemistry: Characterization and Applications of Lanthanide-Binding Biomolecules*; Academic Press, 2021; Vol. 651, pp 193–233.
- (37) Dolg, M. Computational Methods in Lanthanide and Actinide Chemistry; John Wiley & Sons, Ltd., 2015.
- (38) Tanner, P. A. Lanthanide Luminescence in Solids. In Lanthanide Luminescence: Photophysical, Analytical and Biological Aspects; Hänninen, P., Härmä, H., Eds.; Springer Series on Fluorescence; Springer: Berlin, Heidelberg, 2010, pp 183–233.
- (39) Valencia, L.; Martinez, J.; Macías, A.; Bastida, R.; Carvalho, R. A.; Geraldes, C. F. G. C. X-ray Diffraction and ¹H NMR in Solution: Structural Determination of Lanthanide Complexes of a Py₂N₆Ac₄ Ligand. *Inorg. Chem.* **2002**, *41*, 5300–5312.
- (40) Simon, J. D.; Moomaw, W. R.; Ceckler, T. M. The Structure and NMR and Electronic Spectra of Europium(III) Crown Ether Complexes in Solution. *J. Phys. Chem.* **1985**, *89*, 5659–5665.
- (41) Latva, M.; Takalo, H.; Mukkala, V.-M.; Kankare, J. Evaluation of Solution Structures of Highly Luminescent Europium(III) Chelates by Using Laser Induced Excitation of the $^7F_0 \rightarrow ^5D_0$ Transition. *Inorganica Chim. Acta* **1998**, *267*, *63*–72.
- (42) Gateau, C.; Mazzanti, M.; Pécaut, J.; Dunand, F. A.; Helm, L. Solid-State and Solution Properties of the Lanthanide Complexes of a New Nonadentate Tripodal Ligand Derived from 1,4,7-Triazacyclononane. *Dalton Trans.* 2003, 12, 2428–2433.
- (43) Yaita, T.; Narita, H.; Suzuki, Sh.; Tachimori, Sh.; Motohashi, H.; Shiwaku, H. Structural Study of Lanthanides(III) in Aqueous Nitrate and Chloride Solutions by EXAFS. *J. Radioanal. Nucl. Chem.* **1999**, 239, 371–375.
- (44) Shiery, R. C.; Fulton, J. L.; Balasubramanian, M.; Nguyen, M.-T.; Lu, J.-B.; Li, J.; Rousseau, R.; Glezakou, V.-A.; Cantu, D. C. Coordination Sphere of Lanthanide Aqua Ions Resolved with Ab Initio Molecular Dynamics and X-ray Absorption Spectroscopy. *Inorg. Chem.* **2021**, *60*, 3117–3130.

- (45) Allen, P. G.; Bucher, J. J.; Shuh, D. K.; Edelstein, N. M.; Craig, I. Coordination Chemistry of Trivalent Lanthanide and Actinide Ions in Dilute and Concentrated Chloride Solutions. *Inorg. Chem.* **2000**, 39, 595–601.
- (46) Stumpf, S.; Billard, I.; Gaillard, C.; Panak, P. J.; Dardenne, K. TRLFS and EXAFS Investigations of Lanthanide and Actinide Complexation by Triflate and Perchlorate in an Ionic Liquid. *Radiochim. Acta* **2008**, *96*, 1–10.
- (47) Driscoll, D. M.; Shiery, R. C.; Balasubramanian, M.; Fulton, J. L.; Cantu, D. C. Ionic Contraction across the Lanthanide Series Decreases the Temperature-Induced Disorder of the Water Coordination Sphere. *Inorg. Chem.* **2022**, *61*, 287–294.
- (48) Persson, I.; D'Angelo, P.; De Panfilis, S.; Sandström, M.; Eriksson, L. Hydration of Lanthanoid(III) Ions in Aqueous Solution and Crystalline Hydrates Studied by EXAFS Spectroscopy and Crystallography: The Myth of the "Gadolinium Break". *Chem. Eur. J.* **2008**, *14*, 3056–3066.
- (49) Ramírez-Solís, A.; Amaro-Estrada, J. I.; Hernández-Cobos, J.; Maron, L. Aqueous Solvation of SmI_2 : A Born–Oppenheimer Molecular Dynamics Density Functional Theory Cluster Approach. *I. Phys. Chem. A* **2017**, *121*, 2293–2297.
- (50) Yamaguchi, T.; Nomura, M.; Wakita, H.; Ohtaki, H. An Extended X-ray Absorption Fine Structure Study of Aqueous Rare Earth Perchlorate Solutions in Liquid and Glassy States. *J. Chem. Phys.* **1988**, *89*, 5153–5159.
- (51) D'Angelo, P.; Zitolo, A.; Migliorati, V.; Chillemi, G.; Duvail, M.; Vitorge, P.; Abadie, S.; Spezia, R. Revised Ionic Radii of Lanthanoid(III) Ions in Aqueous Solution. *Inorg. Chem.* **2011**, *50*, 4572–4579.
- (52) Kelley, M. P.; Yang, P.; Clark, S. B.; Clark, A. E. Structural and Thermodynamic Properties of the Cm^{III} Ion Solvated by Water and Methanol. *Inorg. Chem.* **2016**, *55*, 4992–4999.
- (53) Ferrier, M. G.; Batista, E. R.; Berg, J. M.; Birnbaum, E. R.; Cross, J. N.; Engle, J. W.; La Pierre, H. S.; Kozimor, S. A.; Lezama Pacheco, J. S.; Stein, B. W.; Stieber, S. C. E.; Wilson, J. J. Spectroscopic and Computational Investigation of Actinium Coordination Chemistry. *Nat. Commun.* **2016**, *7*, 12312.
- (54) Atta-Fynn, R.; Bylaska, E. J.; Schenter, G. K.; de Jong, W. A. Hydration Shell Structure and Dynamics of Curium(III) in Aqueous Solution: First Principles and Empirical Studies. *J. Phys. Chem. A* **2011**, *115*, 4665–4677.
- (55) Atta-Fynn, R.; Bylaska, E. J.; de Jong, W. A. Strengthening of the Coordination Shell by Counter Ions in Aqueous Th⁴⁺ Solutions. *J. Phys. Chem. A* **2016**, *120*, 10216–10222.
- (56) Odoh, S. O.; Bylaska, E. J.; de Jong, W. A. Coordination and Hydrolysis of Plutonium Ions in Aqueous Solution Using Car–Parrinello Molecular Dynamics Free Energy Simulations. *J. Phys. Chem. A* **2013**, *117*, 12256–12267.
- (57) Leung, K.; Nenoff, T. M. Hydration Structures of U(III) and U(IV) Ions from Ab Initio Molecular Dynamics Simulations. *J. Chem. Phys.* **2012**, *137*, 074502.
- (58) Atta-Fynn, R.; Johnson, D. F.; Bylaska, E. J.; Ilton, E. S.; Schenter, G. K.; de Jong, W. A. Structure and Hydrolysis of the U(IV), U(V), and U(VI) Aqua Ions from Ab Initio Molecular Simulations. *Inorg. Chem.* **2012**, *51*, 3016–3024.
- (59) D'Angelo, P.; Migliorati, V.; Gibiino, A.; Busato, M. Direct Observation of Contact Ion-Pair Formation in La³⁺ Methanol Solution. *Inorg. Chem.* **2022**, *61*, 2932.
- (60) Moreau, J.; Guillon, E.; Pierrard, J.-C.; Rimbault, J.; Port, M.; Aplincourt, M. Complexing Mechanism of the Lanthanide Cations Eu³⁺, Gd³⁺, and Tb³⁺ with 1,4,7,10-Tetrakis(carboxymethyl)-1,4,7,10-Tetraazacyclododecane (dota)—Characterization of Three Successive Complexing Phases: Study of the Thermodynamic and Structural Properties of the Complexes by Potentiometry, Luminescence Spectroscopy, and EXAFS. *Chem. Eur. J.* **2004**, *10*, 5218–5232.
- (61) Taube, F.; Drobot, B.; Rossberg, A.; Foerstendorf, H.; Acker, M.; Patzschke, M.; Trumm, M.; Taut, S.; Stumpf, T. Thermodynamic and Structural Studies on the Ln(III)/An(III) Malate Complexation. *Inorg. Chem.* **2019**, *58*, 368–381.

- (62) Cocalia, V. A.; Jensen, M. P.; Holbrey, J. D.; Spear, S. K.; Stepinski, D. C.; Rogers, R. D. Identical Extraction Behavior and Coordination of Trivalent or Hexavalent f-Element Cations Using Ionic Liquid and Molecular Solvents. *Dalton Trans.* **2005**, *11*, 1966–1971.
- (63) Narita, H.; Yaita, T.; Suzuki, S.; Takai, K.; Tachimori, S.; Motohashi, H. Structural studies of lanthanide(III) complexes with oxydiacetic acid and iminodiacetic acid in aqueous solution by EXAFS. *J. Synchrotron Rad.* **2001**, *8*, 672–673.
- (64) Kaliakin, D. S.; Sobrinho, J. A.; Monteiro, J. H. S. K.; de Bettencourt-Dias, A.; Cantu, D. C. Solution Structure of a Europium—Nicotianamine Complex Supports That Phytosiderophores Bind Lanthanides. *Phys. Chem. Chem. Phys.* **2021**, 23, 4287–4299.
- (65) Bhattacharyya, A.; Leoncini, A.; Egberink, R. J. M.; Mohapatra, P. K.; Verma, P. K.; Kanekar, A. S.; Yadav, A. K.; Jha, S. N.; Bhattacharyya, D.; Huskens, J.; Verboom, W. First Report on the Complexation of Actinides and Lanthanides Using 2,2',2"-(((1,4,7-Triazonane-1,4,7-Triyl)Tris(2-Oxoethane-2,1-Diyl)) Tris(Oxy)) Tris(N,N-Dioctylacetamide): Synthesis, Extraction, Luminescence, EXAFS, and DFT Studies. *Inorg. Chem.* 2018, 57, 12987–12998.
- (66) Toraishi, T.; Farkas, I.; Szabó, Z.; Grenthe, I. Complexation of Th(IV) and Various Lanthanides(III) by Glycolic Acid; Potentiometric, 13C-NMR and EXAFS Studies. *J. Chem. Soc. Dalton Trans.* **2002**, *20*, 3805–3812.
- (67) Yaita, T.; Tachimori, S.; Edelstein, N. M.; Bucher, J. J.; Rao, L.; Shuh, D. K.; Allen, P. G. EXAFS studies of americium(III)-benzimidazole complex in ethanol. *J. Synchrotron Rad.* **2001**, 8, 663–665.
- (68) Deblonde, G. J.-P.; Kelley, M. P.; Su, J.; Batista, E. R.; Yang, P.; Booth, C. H.; Abergel, R. J. Spectroscopic and Computational Characterization of Diethylenetriaminepentaacetic Acid/Transplutonium Chelates: Evidencing Heterogeneity in the Heavy Actinide(III) Series. *Angew. Chem., Int. Ed.* **2018**, *57*, 4521–4526.
- (69) Aupiais, J.; Bonin, L.; Den Auwer, C. D.; Moisy, P.; Siberchicot, B.; Topin, S. On the Use of Speciation Techniques and Ab Initio Modelling to Understand Tetravalent Actinide Behavior in a Biological Medium: An^{IV}DTPA Case. *Dalton Trans.* **2016**, 45, 3759–3770.
- (70) Lahrouch, F.; Siberchicot, B.; Fèvre, J.; Leost, L.; Aupiais, J.; Solari, P. L.; Den Auwer, C.; Di Giorgio, C. Carboxylate- and Phosphonate-Modified Polyethylenimine: Toward the Design of Actinide Decorporation Agents. *Inorg. Chem.* **2020**, *59*, 128–137.
- (71) He, X.; Tian, G.; Chen, J.; Rao, L. Characterization of the Extracted Complexes of Trivalent Lanthanides with Purified Cyanex 301 in Comparison with Trivalent Actinide Complexes. *Dalton Trans.* **2014**, *43*, 17352–17357.
- (72) Onghena, B.; Papagni, E.; Souza, E. R.; Banerjee, D.; Binnemans, K.; Vander Hoogerstraete, T. V. Speciation of Lanthanide Ions in the Organic Phase after Extraction from Nitrate Media by Basic Extractants. *RSC Adv.* **2018**, *8*, 32044–32054.
- (73) Vander Hoogerstraete, T.; Souza, E. R.; Onghena, B.; Banerjee, D.; Binnemans, K. Mechanism for Solvent Extraction of Lanthanides from Chloride Media by Basic Extractants. *J. Solut. Chem.* **2018**, *47*, 1351–1372.
- (74) Jensen, M. P.; Bond, A. H. Comparison of Covalency in the Complexes of Trivalent Actinide and Lanthanide Cations. *J. Am. Chem. Soc.* **2002**, *124*, 9870–9877.
- (75) Guoxin, T.; Yongjun, Z.; Jingming, X.; Ping, Z.; Tiandou, H.; Yaning, X.; Jing, Z. Investigation of the Extraction Complexes of Light Lanthanides(III) with Bis(2,4,4-Trimethylpentyl)Dithiophosphinic Acid by EXAFS, IR, and MS in Comparison with the Americium(III) Complex. *Inorg. Chem.* **2003**, *42*, 735–741.
- (76) Brigham, D. M.; Ivanov, A. S.; Moyer, B. A.; Delmau, L. H.; Bryantsev, V. S.; Ellis, R. J. Trefoil-Shaped Outer-Sphere Ion Clusters Mediate Lanthanide(III) Ion Transport with Diglycolamide Ligands. *J. Am. Chem. Soc.* **2017**, *139*, 17350–17358.
- (77) Hall, G. B.; Holfeltz, V. E.; Campbell, E. L.; Boglaienko, D.; Lumetta, G. J.; Levitskaia, T. G. Evolution of Acid-Dependent Am³⁺

- and Eu³⁺ Organic Coordination Environment: Effects on the Extraction Efficiency. *Inorg. Chem.* **2020**, *59*, 4453–4467.
- (78) Verma, P. K.; Mohapatra, P. K.; Yadav, A. K.; Jha, S. N.; Bhattacharyya, D.; Leoncini, A.; Huskens, J.; Verboom, W. Role of Diluent in the Unusual Extraction of Am³⁺ and Eu³⁺ Ions with Benzene-Centered Tripodal Diglycolamides: Local Structure Studies Using Luminescence Spectroscopy and XAS. *New J. Chem.* **2021**, *45*, 16794–16803.
- (79) Ellis, R. J.; Brigham, D. M.; Delmau, L.; Ivanov, A. S.; Williams, N. J.; Vo, M. N.; Reinhart, B.; Moyer, B. A.; Bryantsev, V. S. "Straining" to Separate the Rare Earths: How the Lanthanide Contraction Impacts Chelation by Diglycolamide Ligands. *Inorg. Chem.* **2017**, *56*, 1152–1160.
- (80) Yaita, T.; Narita, H.; Suzuki, S.; Tachimori, S.; Shiwaku, H.; Motohashi, H. Structural Study of Holmium (III) and Uranium (VI) Organic Ligand Complexes by Extended X-Ray Absorbtion Fine-Structure Spectroscopy. *J. Alloys Compd.* **1998**, 271–273, 184–188.
- (81) Simonnet, M.; Kobayashi, T.; Shimojo, K.; Yokoyama, K.; Yaita, T. Study on Phenanthroline Carboxamide for Lanthanide Separation: Influence of Amide Substituents. *Inorg. Chem.* **2021**, *60*, 13409–13418.
- (82) Migliorati, V.; Filipponi, A.; Sessa, F.; Lapi, A.; Serva, A.; D'Angelo, P. Solvation Structure of Lanthanide(III) Bistriflimide Salts in Acetonitrile Solution: A Molecular Dynamics Simulation and EXAFS Investigation. *Phys. Chem. Chem. Phys.* **2019**, *21*, 13058–13069
- (83) Jensen, M. P.; Bond, A. H.; Rickert, P. G.; Nash, K. L. Solution Phase Coordination Chemistry of Trivalent Lanthanide and Actinide Cations with Bis(2,4,4-Trimethylpentyl)Dithiophosphinic Acid. *J. Nucl. Sci. Technol.* **2002**, 39, 255–258.
- (84) Denecke, M. A.; Rossberg, A.; Panak, P. J.; Weigl, M.; Schimmelpfennig, B.; Geist, A. Characterization and Comparison of Cm(III) and Eu(III) Complexed with 2,6-Di(5,6-Dipropyl-1,2,4-Triazin-3-Yl)Pyridine Using EXAFS, TRFLS, and Quantum-Chemical Methods. *Inorg. Chem.* 2005, 44, 8418–8425.
- (85) Bettencourt Dias, A. B.; Viswanathan, S. Luminescent Ln3+ Nitrobenzoato Complexes: First Examples of Sensitization of Green and Red Emission. *Chem. Commun.* **2004**, *8*, 1024–1025.
- (86) Bettencourt-Dias, A.; Viswanathan, S. Nitro-Functionalization and Luminescence Quantum Yield of Eu(III) and Tb(III) Benzoic Acid Complexes. *Dalton Trans.* **2006**, *34*, 4093–4103.
- (87) Viswanathan, S.; de Bettencourt-Dias, A. 2-Chloro-5-Nitrobenzoato Complexes of Eu(III) and Tb(III) A 1D Coordination Polymer and Enhanced Solution Luminescence. *Inorg. Chem. Commun.* **2006**, *9*, 444–448.
- (88) Viswanathan, S.; de Bettencourt-Dias, A. Eu(III) and Tb(III) Luminescence Sensitized by Thiophenyl-Derivatized Nitrobenzoato Antennas. *Inorg. Chem.* **2006**, *45*, 10138–10146.
- (89) Jorgensen, W. L.; Maxwell, D. S.; Tirado-Rives, J. Development and Testing of the OPLS All-Atom Force Field on Conformational Energetics and Properties of Organic Liquids. *J. Am. Chem. Soc.* **1996**, 118, 11225–11236.
- (90) Pothoczki, S.; Pusztai, L. Intermolecular Orientations in Liquid Acetonitrile: New Insights Based on Diffraction Measurements and All-Atom Simulations. *J. Mol. Liq.* **2017**, 225, 160–166.
- (91) Doherty, B.; Zhong, X.; Gathiaka, S.; Li, B.; Acevedo, O. Revisiting OPLS Force Field Parameters for Ionic Liquid Simulations. *J. Chem. Theory Comput.* **2017**, *13*, 6131–6145.
- (92) Baaden, M.; Berny, F.; Madic, C.; Wipff, G. M3+ Lanthanide Cation Solvation by Acetonitrile: The Role of Cation Size, Counterions, and Polarization Effects Investigated by Molecular Dynamics and Quantum Mechanical Simulations. *J. Phys. Chem. A* **2000**, *104*, 7659–7671.
- (93) Berendsen, H. J. C.; Postma, J. P. M.; van Gunsteren, W. F.; DiNola, A.; Haak, J. R. Molecular Dynamics with Coupling to an External Bath. *J. Chem. Phys.* **1984**, *81*, 3684–3690.
- (94) Essmann, U.; Perera, L.; Berkowitz, M. L.; Darden, T.; Lee, H.; Pedersen, L. G. A Smooth Particle Mesh Ewald Method. *J. Chem. Phys.* **1995**, *103*, 8577–8593.

- (95) Abraham, M. J.; Murtola, T.; Schulz, R.; Páll, S.; Smith, J. C.; Hess, B.; Lindahl, E. GROMACS: High Performance Molecular Simulations through Multi-Level Parallelism from Laptops to Supercomputers. *SoftwareX* **2015**, *1*–2, 19–25.
- (96) Perdew, J. P.; Burke, K.; Ernzerhof, M. Generalized Gradient Approximation Made Simple. *Phys. Rev. Lett.* **1996**, *77*, 3865–3868.
- (97) Kühne, T. D.; Iannuzzi, M.; Del Ben, M.; Rybkin, V. V.; Seewald, P.; Stein, F.; Laino, T.; Khaliullin, R. Z.; Schütt, O.; Schiffmann, F.; Golze, D.; Wilhelm, J.; Chulkov, S.; Bani-Hashemian, M. H.; Weber, V.; Borštnik, U.; Taillefumier, M.; Jakobovits, A. S.; Lazzaro, A.; Pabst, H.; Müller, T.; Schade, R.; Guidon, M.; Andermatt, S.; Holmberg, N.; Schenter, G. K.; Hehn, A.; Bussy, A.; Belleflamme, F.; Tabacchi, G.; Glöß, A.; Lass, M.; Bethune, I.; Mundy, C. J.; Plessl, C.; Watkins, M.; VandeVondele, J.; Krack, M.; Hutter, J. CP2K: An Electronic Structure and Molecular Dynamics Software Package Quickstep: Efficient and Accurate Electronic Structure Calculations. J. Chem. Phys. 2020, 152, 194103.
- (98) VandeVondele, J.; Krack, M.; Mohamed, F.; Parrinello, M.; Chassaing, T.; Hutter, J. Quickstep: Fast and Accurate Density Functional Calculations Using a Mixed Gaussian and Plane Waves Approach. *Comput. Phys. Commun.* **2005**, *167*, 103–128.
- (99) Goedecker, S.; Teter, M.; Hutter, J. Separable Dual-Space Gaussian Pseudopotentials. *Phys. Rev. B* **1996**, *54*, 1703–1710.
- (100) VandeVondele, J.; Hutter, J. Gaussian Basis Sets for Accurate Calculations on Molecular Systems in Gas and Condensed Phases. *J. Chem. Phys.* **2007**, *127*, 114105.
- (101) Lu, J.-B.; Cantu, D. C.; Nguyen, M.-T.; Li, J.; Glezakou, V.-A.; Rousseau, R. Norm-Conserving Pseudopotentials and Basis Sets To Explore Lanthanide Chemistry in Complex Environments. *J. Chem. Theory Comput.* **2019**, *15*, 5987–5997.
- (102) Grimme, S.; Antony, J.; Ehrlich, S.; Krieg, H. A consistent and accurate ab initio parametrization of density functional dispersion correction (DFT-D) for the 94 elements H-Pu. *J. Chem. Phys.* **2010**, 132, 2344.
- (103) Nosé, S. A Unified Formulation of the Constant Temperature Molecular Dynamics Methods. *J. Chem. Phys.* **1984**, *81*, 511–519.
- (104) Nosé, S. A Molecular Dynamics Method for Simulations in the Canonical Ensemble. *Mol. Phys.* **1984**, *52*, 255–268.
- (105) Iwasawa, Y.; Asakura, K.; Tada, M. XAFS Techniques for Catalysts, Nanomaterials, and Surfaces; Springer International Publishing Switzerland, 2017.
- (106) Palmer, B. J.; Pfund, D. M.; Fulton, J. L. Direct Modeling of EXAFS Spectra from Molecular Dynamics Simulations. *J. Phys. Chem.* **1996**, *100*, 13393–13398.
- (107) Ankudinov, A. L.; Ravel, B.; Rehr, J. J.; Conradson, S. D. Real-Space Multiple-Scattering Calculation and Interpretation of X-ray-Absorption Near-Edge Structure. *Phys. Rev. B* **1998**, *58*, 7565–7576. (108) Rehr, J. J.; Kas, J. J.; Prange, M. P.; Sorini, A. P.; Takimoto, Y.; Vila, F. Ab Initio Theory and Calculations of X-Ray Spectra. *Comptes Rendus Phys* **2009**, *10*, 548–559.
- (109) Rehr, J. J.; Albers, R. C. Theoretical Approaches to X-Ray Absorption Fine Structure. Rev. Mod. Phys. 2000, 72, 621-654.
- (110) Driscoll, D. M.; Shiery, R. C.; D'Annunzio, N.; Boglaienko, D.; Balasubramanian, M.; Levitskaia, T. G.; Pearce, C. I.; Govind, N.; Cantu, D. C.; Fulton, J. L. Water Defect Stabilizes the Bi³⁺ Lone-Pair Electronic State Leading to an Unusual Aqueous Hydration Structure. *Inorg. Chem.* **2022**, *61*, 14987–14996.
- (111) Basset, J.; Denney, R. C.; Jeffery, G. H.; Mendham, J. Vogel's Textbook of Quantitative Inorganic Analysis, 4th ed.; John Wiley & Sons, Inc., 1978.
- (112) Ravel, B.; Newville, M. ATHENA, ARTEMIS, HEPHAES-TUS: data analysis for X-ray absorption spectroscopy using IFEFFIT. *J. Synchrotron Radiat.* **2005**, *12*, 537–541.
- (113) Ravel, B. Quantitative EXAFS Analysis. In X-Ray Absorption and X-Ray Emission Spectroscopy; John Wiley & Sons, Ltd, 2016, pp 281–302.
- (114) Xia, Q.-Y.; Feng, M.-Y.; Ma, D.-X.; Shi, S.-M.; Xie, Y.-C.; Tian, W.; Shi, H.-J.; Wang, Q.-L.; Wang, W.-M. Structures, Luminescent

- Properties and Magnetic Refrigeration of Two Series of $\rm Ln_2^{III}$ Compounds. *Polyhedron* **2019**, *166*, 141–145.
- (115) Bünzli, J.-C. G.; Yersin, J.-R. Spectroscopic Investigation of Europium(III) Nitrato Complexes in Anhydrous and Aqueous Acetonitrile. *Inorganica Chim. Acta* 1984, 94, 301–308.
- (116) Rao, L.; Tian, G. Complexation of Lanthanides with Nitrate at Variable Temperatures: Thermodynamics and Coordination Modes. *Inorg. Chem.* **2009**, *48*, 964–970.
- (117) Dobler, M.; Guilbaud, P.; Dedieu, A.; Wipff, G. Interaction of Trivalent Lanthanide Cations with Nitrate Anions: A Quantum Chemical Investigation of Monodentate/Bidentate Binding Modes. *New J. Chem.* **2001**, 25, 1458–1465.
- (118) Rudolph, W. W.; Irmer, G. Hydration and Ion Pair Formation in Common Aqueous La(III) Salt Solutions a Raman Scattering and DFT Study. *Dalton Trans.* **2014**, *44*, 295–305.
- (119) Thatipamula, K. C.; Bhargavi, G.; Rajasekharan, M. V. Structural Trends in a 3d-4f System: $Ln(NO_3)_3-Cu(2,2-bipyridine)_2(NO_3)_2$ (Ln=La-Nd, Sm-Yb). ChemistrySelect **2019**, 4, 3450–3458.
- (120) Leverd, P. C.; Nierlich, M. CCDC 103157: Experimental Crystal Structure Determination, 1998.
- (121) Martínez-Sánchez, J. M.; Bastida, R.; Macías, A.; Pérez-Lourido, P.; Valencia, L. Lanthanide(III) Nitrate Complexes with a Tetramethyl 4-(Methyl)Benzoate Pendant-Armed Hexaazamacrocyclic Ligand. *Inorganica Chim. Acta* 2011, 378, 127–133.
- (122) Djanashvili, K.; Platas-Iglesias, C.; Peters, J. A. The Structure of the Lanthanide Aquo Ions in Solution as Studied by ¹⁷O NMR Spectroscopy and DFT Calculations. *Dalton Trans.* **2008**, *5*, 602–607.
- (123) van Loon, A. M.; van Bekkum, H.; Peters, J. A. Structures of Dysprosium(III) Triflates in Water, Methanol, and 2-Propanol As Studied by ¹⁷O and ¹⁹F NMR Spectroscopy. *Inorg. Chem.* **1999**, *38*, 3080–3084.
- (124) Migliorati, V.; Serva, A.; Sessa, F.; Lapi, A.; D'Angelo, P. Influence of Counterions on the Hydration Structure of Lanthanide Ions in Dilute Aqueous Solutions. *J. Phys. Chem. B* **2018**, 122, 2779–2791.
- (125) Ayers, K. M.; Schley, N. D.; Ung, G. Solid State Structures, Solution Behavior, and Luminescence of Simple Tetrakis(2-Pyridylmethyl)Ethylenediamine Lanthanide Complexes. *Eur. J. Inorg. Chem.* **2019**, 2019, 3769–3775.
- (126) Le Borgne, T. L.; Altmann, P.; André, N.; Bünzli, J.-C. G.; Bernardinelli, G.; Morgantini, P.-Y.; Weber, J.; Piguet, C. Tuning Facial—Meridional Isomerisation in Monometallic Nine-Co-Ordinate Lanthanide Complexes with Unsymmetrical Tridentate Ligands. *Dalton Trans.* **2004**, *5*, 723–733.
- (127) Ayers, K. M.; Schley, N. D.; Ung, G. Circularly Polarized Luminescence from Enantiopure C2-Symmetrical Tetrakis(2-Pyridylmethyl)-1,2-Diaminocyclohexane Lanthanide Complexes. *Inorg. Chem.* **2020**, *59*, 7657–7665.
- (128) Sannasy, D.; Marques, H. M.; Fernandes, M. A.; de Sousa, A. S. de. Outer-Sphere Anion Recognition by a Cyclen-Based Octadentate Europium(III) Complex: pH Dependent Recognition of Ortho-Phthalic Acid. *Chem. Commun.* **2014**, *50*, 1582–1584.
- (129) Newville, M. Fundamentals of XAFS. Rev. Mineral. Geochem. 2014, 78, 33-74.
- (130) Hui, Y.; Webster, R. D. Absorption of Water into Organic Solvents Used for Electrochemistry under Conventional Operating Conditions. *Anal. Chem.* **2011**, *83*, 976–981.